Kinetics and Catalysis, Vol. 41, No. 6, 2000, pp. 816–825. Translated from Kinetika i Kataliz, Vol. 41, No. 6, 2000, pp. 897–906.

Zirconium-Containing Compositions with a Component Ratio Characteristic of the Garnet Structure: Physicochemical and Catalytic Properties

A. S. Ivanova, M. V. Mikhan', G. M. Alikina, G. S. Litvak, E. M. Moroz, and E. B. Burgina

Boreskov Institute of Catalysis, Siberian Division, Russian Academy of Sciences, Novosibirsk, 630090 Russia

Received July 30, 1999

Abstract—The possibility for the formation of garnet structures in the Mn–Fe–Zr–O and Ca–Sm–Zr–O systems obtained by the precipitation of the corresponding salts is studied. It is shown that, in the Mn–Fe–Zr–O system, garnet is crystallized at 860–920°C, for which probable cation distribution is estimated to be $\{Zr^{4+}_{2.5}\,Mn^{2+}_{0.5}\}[Mn^{2+}_{2}](Fe^{3+}_{2.5}\,Mn^{3+}_{0.5})O_{12}$. In the Ca–Sm–Zr–O system, the perovskite $CaZrO_3$, pyrochlore $Sm_2Zr_2O_7$, and CaO are formed at 900–1200°C, but compounds with garnet structures are not found. The reported systems are characterized by surface areas of 300–450 m^2/g at ≤450°C, and they have the polydisperse distribution of pores over sizes. The introduction of surfactants at the stage of component mixing enables an increase in the overall pore volume and mechanical strength of these systems. The Mn–Fe–Zr and Ca–Sm–Zr compositions are active catalysts for the complete oxidation of hydrocarbons.

INTRODUCTION

Garnets attract attention due to the specific features of their crystal structure, which is characterized by a cubic elementary cell containing eight formula units $\{A_3\}[B_2](C_3)O_{12}$, where { }, [ ], and () correspond to dodecahedron, octahedron, and tetrahedron cationic positions, respectively [1]. The presence of three nonequivalent positions in the structure opens new avenues for organizing different coordination environments for cations that could be used to construct compositions with the desired physicochemical and catalytic properties.

Much data has been published on silicon-containing garnets [2, 3]. However, garnets with zirconium instead of silicon are of equal interest. Zirconium has a larger coordination number than silicon, and its introduction instead of silicon can change the distribution of cations over interstices in the closest cubic packing of oxygen anions and increase the thermal stability of the compositions. M(II) and M(III) can either be $Mn^{2+}$and Fe^{3+} or Ca^{2+} and Sm^{3+}, the addition of which can lead to a change in the catalytic properties of systems thus obtained in the corresponding reactions. The goal of this work is to study the possibility for the formation of garnet in the Mn–Fe–Zr–O and Ca–Sm–Zr–O systems obtained by precipitation and to test physicochemical and catalytic properties of these systems in the complete oxidation of hydrocarbons.

EXPERIMENTAL

The samples of ternary zirconium-containing systems were prepared by several methods.

Mn–Fe–Zr–O System

Method I. The system was prepared by precipitation from a solution of manganese, iron, and zirconium nitrates by adding an aqueous solution of KOH (2 mol/l) until pH 9 with further aging via two stages: (1) stirring at room temperature for 30 min and (2) stirring at 100°C for 2 h.

Method II. The system was prepared by precipitation from the solution of manganese, iron, and zirconium nitrates. For that, an aqueous solution of KOH (2 mol/l) was titrated by the solution of these salts to pH 9. The aging stage was analogous to that in method I.

Method III. The system was prepared by precipitation from the solution of manganese, iron, and zirconium nitrates by adding an aqueous solution of KOH (2 mol/l) at a constant pH (pH 9). The aging stage was analogous to that in method I.

Method IV. The system was prepared by precipitation from the solution of manganese, iron, and zirconium nitrates by adding an aqueous solution of NH_4OH (1 : 1) at a constant pH (pH 9). The aging stage was analogous to that in method I.

To test the effect of a reducing agent added during precipitation on the subsequent stages of the formation of composite oxide systems, a sample was prepared with H_2O_2 added (method IA).

Ca–Sm–Zr–O System

This system was prepared by consecutive precipitation of samarium and zirconium nitrates at pH 9 (aging at room temperature for 30 min) and then calcium

0023-1584/00/4106-0816$25.00 © 2000 MAIK "Nauka /Interperiodica"

nitrate at pH 11.5 by KOH (2 mol/l) (aging at 100°C for 2 h).

All suspensions were filtered and precipitates were washed out with distilled water until nitrates disappeared from the filtered mass. The samples were dried in air at room temperature, then at 110°C for 12 h, and calcined in air at 250–1200°C.

For comparison, we also prepared binary systems with component ratios corresponding to the ternary systems. Mn–Fe–O, Mn–Zr–O, Fe–Zr–O, and Sm–Zr–O were prepared by coprecipitation from a mixture of corresponding nitrates by an aqueous solution of KOH. Ca–Sm–O and Ca–Zr–O were prepared by consecutive precipitation of a mixture from the corresponding nitrates by adding the necessary amount of KOH. Aging, drying, and thermal treatment stages were analogous.

The porous structure in some samples was controlled by adding surfactants both at the stage of precipitation and mixing of preliminarily synthesized and dried samples. Cellulose with particle sizes of ≤0.25 mm, carboxymethylcellulose, and polyvinyl alcohol were used as surfactants. The concentration of surfactants in all samples was 1% based on oxides.

The concentrations of the main components were determined by the atomic-adsorption method [4]. Thermal analysis was carried out using a Q-1500D instrument at 18–1200°C at a heating rate of 10°C/min. The catalyst sample weighed 0.2 g. The calculation of apparent kinetic parameters was performed using thermal analysis data obtained under comparable conditions. The catalyst loading weight was 0.1 g, and the accuracy in determining a weight loss was ±0.5%. X-ray phase analyses were carried out using an HZG-4C diffractometer with a monochromatic CuK_α irradiation. The accuracy in determining the unit-cell parameter of the solid solution was ±0.003 Å. The size of the regions of coherent scattering D was calculated by the Selyakov–Shearer formula [5]. The IR spectra of samples were recorded using an IR Fourier-transform MV-102 spectrometer at room temperature. The samples were prepared by tableting of a 2-mg sample with KBr.

The total specific surface areas of the samples were determined by the method of argon thermal desorption [6]. The error of this method is ±10%. The porous structure was analyzed using mercury porosimetry using a Pore Sizer 9300 instrument. The mechanical crushing strength was measured using an MP-9C instrument. In the calculations, we averaged the results over 20 granules.

The catalytic properties of samples were studied in the following reactions:

(1) Selective nitrogen oxide reduction by propane in an oxidative medium. The conversion of nitrogen oxide and the conversions of propane into CO and CO_2 were estimated for the standard composition of the mixture (0.1 vol % NO, 0.13 vol % C_3H_8, 1 vol % O_2, and balance helium) in a flow-type setup at a space velocity of 4000 h^{-1} at 250–700°C. The concentrations of all components were determined by chromatography.

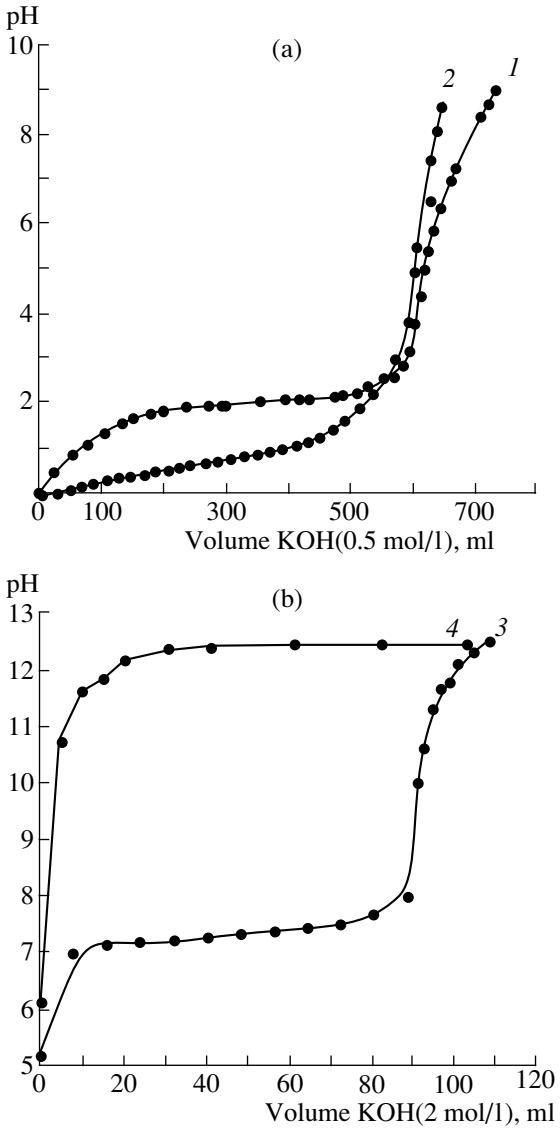

Fig. 1. Potentiometric titration curves of 0.5-mol/l solutions: (*1*) $Fe(NO_3)_3$, (*2*) $ZrO(NO_3)_2$, (*3*) $Sm(NO_3)_3$, and (*4*) $Ca(NO_3)_2$ by a KOH solution with a concentration of (*1*, *2*) 0.5 mol/l and (*3*, *4*) 2 mol/l.

(2) The complete oxidation of butane in a flow-circulation setup. The concentration of butane in a butane–air mixture was 0.5 vol %. Tests were performed in a fixed bed over grains with a size of 1.0–2.0 mm and granules larger than 15 mm at 400°C. The initial reactants and reaction products were analyzed by chromatography. The conversion of butane was 60%. The degree of catalyst utilization was calculated as the ratio of the granulated sample activity to the activity of the same sample in the form of a certain fraction.

Table 1. Effect of the preparation procedure on the chemical composition of zirconium-containing samples

Preparation procedure	Chemical composition,* mol %	
	calculation	experiment
	$MnO–Fe_2O_3–ZrO_2$	
I	41.4 : 15.3 : 43.3	37.6 : 18.3 : 44.0
II	″	37.0 : 17.8 : 45.2
III	″	36.5 : 17.1 : 46.4
IV	″	33.0 : 18.8 : 48.2
	$CaO–Sm_2O_3–ZrO_2$	
–	44.7 : 12.3 : 43.0	51.2 : 7.9 : 40.9

* The concentration of potassium in the Mn–Fe–Zr–O and Ca–Sm–Zr–O samples was at most 0.01 and 0.4%, respectively.

Table 2. Thermal analysis data for the systems under study

System	Preparation procedure	*T*, °C (Δ*m*, wt %)	
		endo-effects	*exo*-effects
Mn–Fe–Zr–O	I	130 (25.0)	240 (0.0), 320 (0.9)
		1190 (0.0)	415 (1.4), 690 (1.1)
			860 (0.8)
″	II	140 (23.3)	240 (0.0), 320 (0.9)
		1195 (0.5)	440 (0.6), 700 (1.3)
			875 (1.0)
″	III	135 (22.8)	235 (0.0), 315 (1.0)
		1195 (0.5)	425 (1.5), 695 (0.3)
			875 (0.5)
″	IV	130 (32.5)	235 (0.0), 315 (1.2)
		1180 (0.0)	395 (1.5), 700 (0.7)
			925 (0.5)
Ca–Sm–Zr–O	–	150 (10.7)	–
		360 (1.0)	
		560 (2.3)	
		845 (9.5)	

RESULTS AND DISCUSSION

According to [7–9], the synthesis of garnet by the precipitation method is favorable for the formation of its structure at a lower temperature than in the solid-phase synthesis. The higher the degree of homogeneity achieved at the precipitation stage, the lower the crystallization temperature. For the systems under study, the choice of a precipitation method is determined by comparing the values of pH corresponding to the precipitation of respective components. Figure 1 shows that pH at which iron and zirconium hydroxides start to precipitate differ only slightly: 1.5 and 2.0, respectively. Manganese precipitates with a first drop of a precipitation agent because it is an easily precipitating hydroxide [10]. Therefore, the Mn–Fe–Zr–O samples were prepared by several methods (Table 1). For the Ca–Sm–Zr–O systems, the difference in precipitation pH for the corresponding components (Fig. 1) is substantial, and only consecutive precipitation is possible. This led to a lower degree of homogeneity of the synthesized samples.

Table 1 shows that, of all methods for the preparation of the Mn–Fe–Zr–O samples, method I provides a chemical composition that is the closest to the calculated one. For the samples synthesized by method IV, the deviation is the greatest. Substantial deviations of calculated and experimental chemical compositions were observed for the Ca–Sm–Zr–O sample.

Thermal analysis of the Mn–Fe–Zr–O samples showed that methods I–III virtually do not affect the positions of thermal effects, and a shift of some peaks (Table 2) are only observed for the samples prepared by the precipitation with NH_4OH (method IV). The low-temperature endo-effect at 130–140°C is stipulated by the removal of unbound water. The exo-effects at 235–700°C are probably associated with the crystallization of iron, manganese, and zirconium oxides, or with the formation of solid solutions based on these oxides. The high-temperature exo-effect at 860–925°C probably refers to the crystallization of the compound with a garnet structure [7]. The endo-effects at 1180–1195°C refer to a polymorphic transition of γ-Mn_2O_3 into β-Mn_2O_3 [11].

The presence of low-temperature and high-temperature endo-effects (Table 2) stipulated by the removal of unbound water (150°C) and possibly by the stepwise dehydration of samarium and calcium hydroxides with the formation of a pyrochlore structure (360–845°C) [12–14] is characteristic of the thermal decomposition of the Ca–Sm–Zr–O sample. High-temperature exo-effects are absent.

X-ray phase analyses of the Mn–Fe–Zr–O samples (Table 3) demonstrated that they remain X-ray amorphous up to 750°C; the main phase of the sample calcined at 750°C is cubic ZrO_2 with a unit-cell parameter equal to 4.99 Å vs. 5.09 Å for pure ZrO_2, which is probably due to the inclusion of Fe^{3+} or Mn^{3+} into the struc-

Table 3. X-ray phase analysis of Mn–Fe–Zr–O samples

System	Treatment temperature, °C	X-ray phase analysis data		
		phase	unit-cell parameter, Å	*D*, Å
Mn–Fe–Zr–O	110	amorphous	–	–
″	250	amorphous	–	–
″	350	amorphous	–	–
″	450	amorphous	–	–
″	750	cubic ZrO_2	4.99	45
		α-Fe_2O_3 (traces)	–	–
″	900	tetragonal ZrO_2	–	–
		monoclinic ZrO_2	–	–
		α-Fe_2O_3	*	–
		β-Mn_2O_3	9.411	400
″	1200	monoclinic ZrO_2	–	500
		β-Mn_2O_3	9.411	–
		garnet	11.240	–
Fe–Mn–O	450	$(Fe,Mn)_3O_4$	8.346	85
		γ-Mn_2O_3	–	–
″	730	α-Fe_2O_3	*	–
		β-Mn_2O_3	9.411	350
Mn–Zr–O	450	amorphous	–	–
″	750	cubic ZrO_2	5.055	45
Fe–Zr–O	450	amorphous	–	–
		α-Fe_2O_3	*	200
″	850	monoclinic ZrO_2	–	–
		α-Fe_2O_3	*	1000

* a = 5.040 Å, c = 13.740 Å [15].

ture of ZrO_2 ($r_{Zr^{4+}}$ = 0.82 Å, $r_{Fe^{3+}}$ = 0.67 Å, $r_{Mn^{3+}}$ = 0.70 Å, and $r_{Mn^{2+}}$ = 0.91 Å). The phase of α-Fe_2O_3 is present in a small amount. Upon heating to 900°C, tetragonal and monoclinic modification of ZrO_2, α-Fe_2O_3, and β-Mn_2O_3 with normal parameters are formed [15]. The formation of β-Mn_2O_3 at a lower temperature than that suggested by thermal analysis data (Table 2) can be due to the thermal treatment regime (isothermal) or to the presence of other components in the system. Also, if we take into account that the tetragonal modification of ZrO_2 is observed in none of the binary systems (Table 3) and that this modification exists in individual ZrO_2 at lower temperatures, the presence of some of its lines in ternary system is probably associated with the formation of a new phase with a set of interplanar distances close to the set of lines in the tetragonal modification. The data of thermal analysis are also supportive of this idea and suggest that a new phase is crystallized at 860–920°C. At 1200°C, changes in the phase composition and the unit-cell parameters of the corresponding phases are observed (Table 3): the α-Fe_2O_3 phase disappears, and a new phase is formed with a line set characteristic of the garnet structure and a unit-cell param-

Table 4. X-ray phase analysis of the Ca–Sm–Zr–O system

System	Treatment temperature, °C	X-ray phase analysis data		
		phase	unit-cell parameter, Å	*D*, Å
Ca–Sm–Zr–O	450	$CaCO_3$ (traces), CaO	–	–
		cubic ZrO_2	5.160	–
″	750	$CaZrO_3$	*	300
		CaO	–	–
		(Zr, Sm)O_2	5.258	25
		$Sm_2Zr_2O_7$ (traces)	–	–
″	750**	$CaZrO_3$	*	300
		CaO	–	–
		(Zr, Sm)O_2	5.232	25
		$Sm_2Zr_2O_7$ (traces)	–	–
″	900	$CaZrO_3$	*	350
		CaO	–	–
		$Sm_2Zr_2O_7$	–	–
″	1400	$CaZrO_3$	*	450
		CaO	–	–
		$Sm_2Zr_2O_7$	–	–
Sm–Zr–O	450	amorphous	–	–
″	750	$Sm_2Zr_2O_7$	10.590	50
		cubic Sm_2O_3	5.464	–
		cubic ZrO_2 (traces)	–	–
Ca–Sm–O	450	$CaCO_3$	–	–
		CaO	–	–
		cubic Sm_2O_3	5.464	80
″	750	CaO	–	–
		cubic Sm_2O_3	5.464	350
Ca–Zr–O	450	amorphous	–	–
		CaO	–	–
		$CaCO_3$	–	–
″	750	$CaZrO_3$	*	300
		cubic ZrO_2	5.14	50
		CaO	*	–

* a = 5.762 Å, b = 8.017 Å, c = 5.591 Å [15].
** Calcination was carried out in a nitrogen flow.

eter of 11.240 Å. The phases of monoclinic ZrO_2 and β-Mn_2O_3 are also present, but their amounts are small.

Table 4 describes the phase composition of the Ca–Sm–Zr–O system. It is seen that, at 450°C, the phases of CaO, $CaCO_3$ (traces) and cubic ZrO_2 are present in addition to the amorphous phase. At 750°C, the perovskite $CaZrO_3$ phase with normal parameters [15] is formed in addition to the above phases, and the beginning of pyrochlore $Sm_2Zr_2O_7$ formation is observed. The $CaCO_3$ phase is not observed. The unit-cell parameter of the solid solution based on cubic ZrO_2 increases and becomes 5.258 Å (Table 4). This fact points to an increase in the fraction of samarium in the structure of ZrO_2 comparatively to that in the sample calcined at 450°C. The thermal treatment of this sample in a nitrogen flow at 750°C did not result in a change in

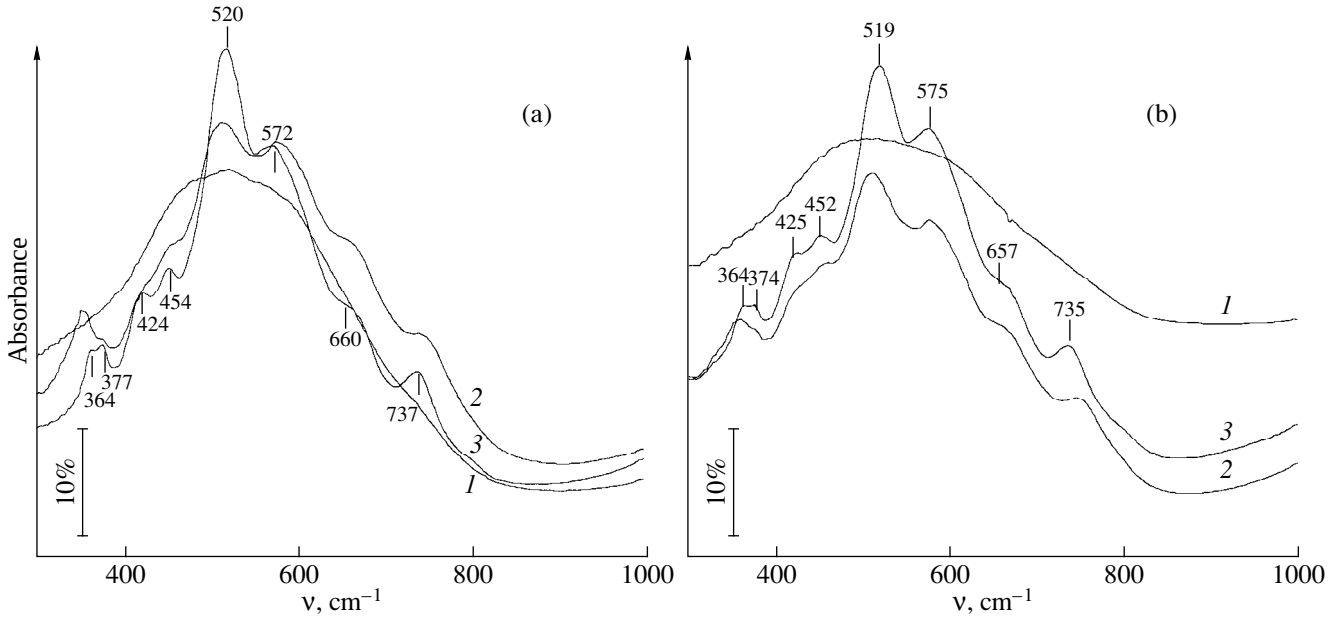

Fig. 2. IR spectra of the Mn–Fe–Zr–O samples obtained by precipitation with (a) KOH and (b) NH_4OH and calcined at (*1*) 700, (*2*) 900, and (*3*) 1200°C.

the phase composition, but the unit-cell parameter of the solid solution based on cubic ZrO_2 somewhat decreased (Table 4). With an increase in the temperature of sample treatment to 900–1400°C, the $(Zr, Sm)O_2$ phase disappears. This is probably due to the fact that this phase is intermediate, and it transforms into the $Sm_2Zr_2O_7$ phase with an increase in temperature by analogy with the Nd–Zr–O and Hf–Dy–O systems [16]. The phase with a garnet structure was not detected (Table 4).

IR spectroscopic study of two samples differing in the preparation procedure and treatment temperature (Fig. 2) provides further evidence for the formation of garnet in the Mn–Fe–Zr–O system. The amount and position of the absorption bands in an IR spectra depends on the sample treatment temperature. The sample calcined at 700°C contains a broad band with a maximum at 523 cm^{-1} (Fig. 2a, curve *1*); at 900°C, it transforms into two absorption bands (520 and 572 cm^{-1}), and new bands appear at 364, 377, 424, 454, 680, and 737 cm^{-1}. The intensities of these bands are low (Fig. 2a, curve *2*). At 1200°C, the intensities of bands increase, especially at 520 and 572 cm^{-1} (Fig. 2a, curve *3*).

Comparison of the results obtained in this work with data reported in [9, 17, 18] led us to conclude that the sample calcined at 700°C is a solid solution based on cubic ZrO_2, because the nature of the IR spectrum and the position of the maximum (523 cm^{-1}) are analogous to those of cubic ZrO_2 [18]. After the thermal treatment at 900°C, the formation of garnet is observed as evident from the appearance of absorption bands at 520 and 572 cm^{-1}, which are the most characteristic of this structure [9, 17]. The appearance of the bands at 364 and 737 cm^{-1} points to the pres-

Table 5. Apparent kinetic parameters of the thermal decomposition of Mn–Fe–Zr–O of the samples determined from the "fixed intervals" of endo/exo effects

Preparation procedure	Kinetic parameters*											
	n_1	E_1	$\log A_1$	n_2	E_2	$\log A_2$	n_3	E_3	$\log A_3$	n_4	E_4	$\log A_4$
	125–145°C			400–450°C			710–730°C			860–920°C		
I	1.18	35.1	3.73	1.43	82.5	4.96	2.18	450.6	22.5	1.69	307.7	12.7
IA	1.20	32.4	3.40	1.65	86.1	5.50	0.94	507.9	26.7	1.59	478.9	20.5
IV	1.18	30.8	3.24	1.05	55.1	3.26	1.93	434.8	21.6	1.17	879.9	38.2

* n_i is the power of the rate law; E_i is the activation energy, kJ/mol, A_i is the preexponential factor, s^{-1}.

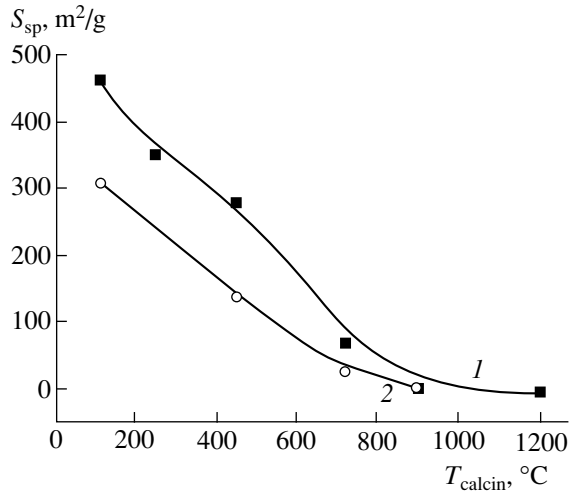

Fig. 3. Specific surface area vs. calcination temperature: (*1*) Mn–Fe–Zr–O and (*2*) Ca–Sm–Zr–O.

ence of monoclinic ZrO_2 [18]. An increase in the calcination temperature to 1200°C is favorable for an increase in the fraction of garnet, while the fraction of monoclinic ZrO_2 is preserved.

Table 6. Enthalpies of changes in the coordination numbers [22]

Ion	Change in the coordination number	ΔH, kJ/mol
Fe^{3+}	6 → 4	22.2
	6 → 5	11.1
Mn^{2+}	6 → 8	28
Mn^{3+}	6 → 4	50
Zr^{4+}	7 → 6	46
	7 → 8	20
Fe^{2+}	6 → 8	50
	6 → 4	20.9

Table 7. Calculated enthalpies of garnet formation from oxides in the Mn–Fe–Zr–O system

x	ΔH, kJ/mol
0.5	–122.85
0.7	–114.73
1.0	–102.55
1.2	–94.43
1.5	–82.25

The IR spectra of Mn–Fe–Zr–O samples precipitated with NH_4OH are analogous to those considered above (Fig. 2b). They differ only in the intensities of bands and this difference is probably due to a difference in the fractions of garnet phase formed in both cases.

This is also evident from the values of apparent kinetic parameters of thermal decomposition for the samples prepared with different precipitation agents (Table 5). These parameters were determined from the thermal analysis data using fixed intervals of endo/exo effects according to [19]. It is seen that the precipitation agent substantially affects the kinetic parameters of garnet crystallization (at T = 860–920°C). Thus, the apparent activation energy of garnet formation has the lowest value when KOH is used, whereas it is the highest in the case of NH_4OH. These facts suggest that KOH is a preferable precipitation agent for the preparation of garnet.

Thus, the results of thermal analysis, X-ray phase analysis, and IR spectroscopic study showed that a compound with a garnet structure is formed in the Mn–Fe–Zr–O system. Taking into account the sizes of the ionic radii of the system components, we can assume that the distribution of cations over the positions of the structure is different than in formula $\{Mn_3\}[Fe_2](Zr_3)O_{12}$.

To find the most probable distribution of cations over interstices in Mn–Fe–Zr–O garnet, we estimated using the Pauling formula [20] that ions such as Fe^{2+}, Mn^{2+}, and Zr^{4+} can occupy dodecahedral and octahedral vacancies in the closest oxygen packing, and Fe^{3+} and Mn^{3+} can occupy octahedral and tetrahedral positions. Proceeding from this fact, the supposed cation distribution over interstices in garnet is

$$\{Mn_x^{2+}Fe_y^{2+}Zr_{3-x-y}^{4+}\}[Zr_z^{4+}Fe_\gamma^{3+}Mn_{2-z-\gamma}^{2+}] \times (Fe_\psi^{3+}Mn_{3-\psi}^{3+})O_{12}.$$

For many composite oxides, the enthalpies of their formation from simple oxides can be calculated using equations of the type $\Delta H = A + B\delta H$ (kJ/mol) where δH is the sum of enthalpies of changing the coordination numbers of cations, and A and B are constants specific for the oxide type [21].

Preferred positions of cations in the structures of oxides are determined by energy differences. Table 6 shows the values of δH for the ions under discussion. It is seen that Zr^{4+} and Mn^{2+} prefer dodecahedrons in this combination of cations, whereas Fe^{2+} does not. Comparison of preference energies (PE) of cation location in octahedrons vs. tetrahedrons [22], PE (kJ/mol): 0 (Mn^{2+}) < 20.9 (Fe^{2+}) ≤ 22.2 (Fe^{3+}) < 50.0 (Mn^{3+}) suggests that Mn^{2+} prefers octahedral positions, Fe^{2+} and Fe^{3+} have about the same preferences, and Mn^{3+} prefers tetrahedral positions.

Taking into account the above data and the phase composition of the Mn–Fe–Zr–O system according to which the monoclinic phase of ZrO_2 and β-Mn_2O_3 are

Table 8. Textural characteristics of the Mn–Fe–Zr–O and Ca–Sm–Zr–O samples

Sample	T_{calcin}, °C	V_{pore}, cm^3/g	Pore volume distribution, cm^3/g				Fraction of pores with $r > 100$ nm, %
			<10 nm	10–100 nm	100–1000 nm	>1000 nm	
Mn–Fe–Zr–O	450	0.102	0.008	0.020	0.010	0.064	63
Mn–Fe–Zr–O	750	0.164	0.012	0.024	0.056	0.072	78
Ca–Sm–Zr–O	450	0.148	0.024	0.076	0.008	0.040	32
Ca–Sm–Zr–O	750	0.250	0.050	0.070	0.065	0.065	52

Table 9. Effect of surfactants and the method of their introduction on the textural characteristics of zirconium-containing systems

Surfactant	Method	T_{calcin}, °C	S_{sp}, m^2/g	V_{pore}, cm^3/g	Pore volume distribution, cm^3/g				Fraction of pores with $r > 100$ nm, %
					<10 nm	10–100 nm	100–1000 nm	>1000 nm	
Mn–Fe–Zr–O									
Cellulose	Precipitation	450	90	0.390	0.040	0.005	0.020	0.325	88
Carboxymethyl-cellulose	Precipitation	450	270	0.083	0.028	0.007	0.011	0.037	58
Carboxymethyl-cellulose	Mixing	450	230	0.290	0.030	0.020	0.140	0.100	83
Cellulose	Precipitation	750	30	0.282	0.022	0.015	0.045	0.200	87
Carboxymethyl-cellulose	Precipitation	750	13	0.150	0.008	0.096	0.012	0.034	31
Carboxymethyl-cellulose	Mixing	750	18	0.300	0.010	0.100	0.150	0.040	63
Ca–Sm–Zr–O									
Polyvinyl alcohol	Precipitation	750	25	0.096	0.034	0.017	0.001	0.038	47
Polyvinyl alcohol	Mixing	750	22	0.320	0.025	0.055	0.130	0.110	65
Carboxymethyl-cellulose	Precipitation	750	27	0.062	0.016	0.060	0.040	0.036	65
Carboxymethyl-cellulose	Mixing	750	12	–	–	–	–	–	–

formed in addition to garnet, the formula of cation distribution over positions in the structure can be simplified:

$$\{Zr^{4+}_{3-x}Mn^{2+}_{x}\}[Fe^{3+}_{2x-1}Mn^{2+}_{3-2x}] \times (Fe^{3+}_{3-x}Mn^{3+}_{x})O_{12}.$$

Using this formula and the correlation equation for garnet $\Delta H = -224 + 0.7\delta H$ kJ/mol [23], we calculated the enthalpies of garnet formation from simple oxides.

Analysis of enthalpies in Table 7 shows that the preferred distribution of cations is ΔH:

$$\{Zr^{4+}_{2.5}Mn^{2+}_{0.5}\}[Mn^{2+}_{2}](Fe^{3+}_{2.5}Mn^{3+}_{0.5})O_{12} \quad (x = 0.5).$$

Zirconium-containing systems calcined at ≤750°C are highly disperse (Tables 3 and 4) because they contain phases with crystallite sizes (D) smaller than 300 Å as determined by X-ray analysis. These data agree with the results of adsorption measurements. Figure 3 shows that the value of the specific surface area of hydroxide

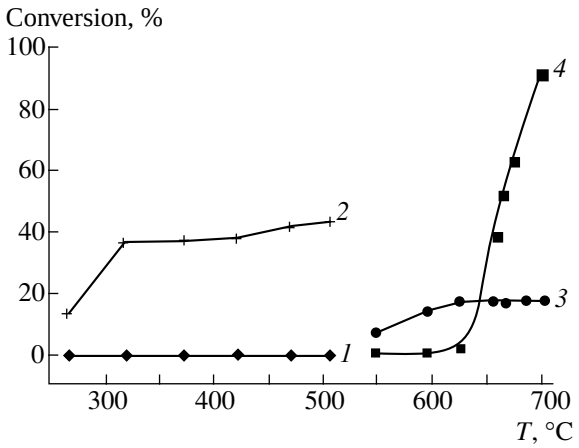

Fig. 4. Activity of samples (*1*, *2*) Mn–Fe–Zr–O and (*3*, *4*) Ca–Sm–Zr–O in (*1*, *3*) nitrogen oxide reduction and (*2*, *4*) propane conversion in the presence of oxygen.

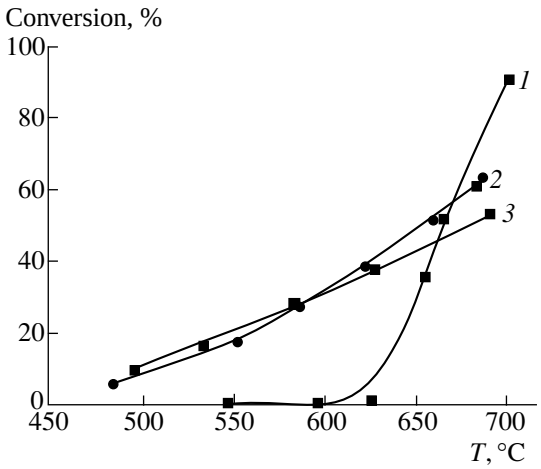

Fig. 5. Propane conversion in the presence of nitrogen oxide and oxygen vs. temperature for binary and ternary samples: (*1*) Ca–Sm–Zr–O, (*2*) Ca–Zr–O, and (*3*) Sm–Zr–O.

zirconium-containing systems varies between 310 and 460 m^2/g. An increase in the calcination temperature is accompanied by a decrease in the specific surface area in the Mn–Fe–Zr–O and Ca–Sm–Zr–O systems due to the formation of low-dispersity phases and sintering. However, the thermal stability of the Mn–Fe–Zr–O system is higher, all other conditions being the same.

Samples calcined at 450 and 750°C are polydisperse, and the fractions of large pores ($r > 100$ nm) in the Mn–Fe–Zr–O and Ca–Sm–Zr–O samples are 63 and 32%, respectively. An increase in the temperature of treatment is accompanied by an increase in the fraction of these pores (Table 8).

The Mn–Fe–Zr–O sample has a small volume of pores and a rather high strength. In contrast, the Ca–Sm–Zr–O sample has a rather large volume of pores (Table 8) and a low strength.

To optimize textural and strength characteristics, we attempt to control the pore structure of the systems by adding surfactants. This led to an increase in the overall pore volume both in the Mn–Fe–Zr–O system (Table 9) and in the Ca–Sm–Zr–O system. The specific surface area changed insignificantly in the case of the Mn–Fe–Zr–O system, and the mechanical strength increased in the case of the Ca–Sm–Zr–O system.

Catalytic properties of zirconium-containing systems were studied in the reaction of nitrogen oxide reduction by propane in an oxidative atmosphere. Figure 4 shows that these systems show low activity in nitrogen oxide reduction, although they are active toward propane transformation into CO_2. The conversion of propane on a Mn–Fe–Zr–O sample reached ~40% even at ~320°C, and the conversion is 90% at 700°C in the case of the Ca–Sm–Zr–O sample. Differences in the behavior of the samples are due to different mechanisms of reac-

Table 10. Catalyst activities in butane oxidation at 400°C

Catalyst	Composition, wt %	T_{calcin}, °C	$W(C_4H_{10}) \times 10^7$, mol g^{-1} s^{-1}		Degree of active component use, %
			granules (<15 mm)	granules (1–2-mm fraction)	
IK-12-1	26% CuO/Al_2O_3	500	2.1	4.9	43
IK-12-2	35% $CuCr_2O_4/Al_2O_3$	500	6.0	24.4	25
IK-12-3	10% CuO/Al_2O_3	500	3.2	7.9	40
IK-12-4	$CuO + Fe_2O_3$	500	10.7	19.4	55
IK-12-7	5% CuO/Al_2O_3	500	1.7	3.0	56
IKT-12-6	30% CuO + 70% Al_2O_3	500	1.2	7.9	16
Mn–Fe–Zr–O	23.4% MnO–24.8% Fe_2O_3–51.8% ZrO_2	750	2.8*	3.5	79

* Granule is a 1-mm-thick ring with an outer diameter of 4 mm.

tions [24]: alkane oxidation occurs via a single-step mechanism at low temperatures (≤500°C), whereas it occurs via several steps at higher temperatures (>650°C). Note that the activity of binary Ca(Sm)–Zr–O samples at >650°C was lower than the activity of the corresponding ternary system (Fig. 5). Therefore, we may conclude that the activity of the Ca–Sm–Zr–O sample is not the sum of binary sample activities but instead depends on the mutual effects of phases involved in the composition.

The Mn–Fe–Zr–O sample was tested in the complete oxidation of butane. Table 10 shows the values of reaction rates for this and other (IK-12-1 through IKT-12-6 [25]) catalysts. It is seen that our sample, calcined at a higher temperature than other catalysts, has an activity comparable to the activities of other samples. A switch from a catalyst with 1–2-mm grains to granules did not lead to a significant decrease in the activity. The use of the Mn–Fe–Zr–O catalyst in the form of rings is favorable for the more efficient use of the active component compared with known catalysts.

REFERENCES

1. Kuzmicheva, G.M., Mukhin, B.V., Khomutova, E.G., *et al., Neorg. Mater.,* 1993, vol. 29, no. 1, p. 89.
2. Beltran, A., Andres, J., Igualada J.A., and Carda, J., *J. Phys. Chem.*, 1995, vol. 99, no. 17, p. 6493.
3. Chalyi, V.P., Makarova, Z.Ya., and Khomenko, I.V., *Ukr. Khim. Zh.*, 1978, vol. 44, no. 9, p. 904.
4. Price, W.J., *Analytical Atomic-Absorption Spectroscopy*, New York: Heyden and Son, 1976.
5. Umanskii, Ya.S., *Rentgenografiya metallov* (X-ray Analysis of Metals), Moscow: Metallurgizdat, 1960, p. 273.
6. Buyanova, N.Ya., Karnaukhov, A.P., and Alabuzhev, Yu.A., *Opredelenie poverkhnosti dispersnykh i poristykh materialov* (Surface Measurements of Disperse and Porous Materials), Novosibirsk: Inst. of Catalysis, 1978.
7. Zinov'ev, C.Yu. and Krzhizhanovskaya, V.A., in *Khimiya i tekhnologiya silikatnykh i tugoplavkikh nemetallicheskikh materialov* (Chemistry and Technology of Silicate and Refractory Materials), Leningrad: Nauka, 1989, p. 67.
8. Mezin, N.I., Kuznetsov, E.N., and Starostyuk, N.D., *Neorg. Mater.,* 1989, vol. 25, no. 7, p. 1187.
9. Chalyi, V.P., Lukachina, E.N., and Simonovich, L.M., *Izv. Akad. Nauk SSSR, Ser. Neorg. Mater.*, 1974, vol. 10, no. 1, p. 2028.
10. Dzis'ko, V.A. and Karnaukhov, A.P., *Fiziko-khimicheskie osnovy sinteza okisnykh katalizatorov* (Physicochemical Foundations of Oxide Catalyst Preparation), Novosibirsk: Nauka, 1978.
11. Tret'yakov, Yu.D., *Termodinamika ferritov* (Thermodynamics of Ferrites), Moscow: Khimiya, 1967.
12. Gavrish, A.M., Gul'ko, N.V., and Tarasova, L.A., *Zh. Neorg. Khim.*, 1981, vol. 26, no. 12, p. 3329.
13. Ivanova, A.S., Moroz, E.M., Litvak, G.S., and Okkel', L.G., *Neorg. Mater.*, 1998, vol. 34, no. 4, p. 432.
14. Ivanova, A.S., Moroz, E.M., and Litvak, G.S., *React. Kinet. Catal. Lett.*, 1998, vol. 65, no. 1, p. 169.
15. *ASTM Diffraction Data Cards and Alphabetical and Grouped Numerical Index of X-ray Diffraction Data*, Philadelphia: ASTM, 1967.
16. Glushkova, V.B. and Keler, E.K., in *Khimiya i tekhnologiya silikatnykh i tugoplavkikh nemetallicheskikh materialov* (Chemistry and Technology of Silicate and Refractory Materials), Leningrad: Nauka, 1989, p. 41.
17. Apte, P., Burke, H., and Pickup, H., *J. Mater. Res.*, 1992, vol. 7, no. 3, p. 706.
18. Ivanova, A.S., *Doctoral (Chem.) Dissertation*, Novosibirsk: Inst. of Catalysis, 1996, p. 364.
19. Brown, M.E., Dollimore, D., and Galwey, A.K., *Comprehensive Chemical Kinetics*, Amsterdam: Elsevier, 1980, p. 196.
20. Pauling, L., *The Nature of the Chemical Bond and the Structure of Molecules and Crystals: An Introduction to Modern Structural Chemistry*, Ithaca: Cornell University Press, 1945.
21. Reznitskii, L.A., *Neorg. Mater.*, 1993, vol. 29, no. 3, p. 386.
22. Reznitskii, L.A., *Zh. Fiz. Khim.*, 1993, vol. 67, no. 12, p. 2379.
23. Reznitskii, L.A., *Zh. Fiz. Khim.*, 1987, vol. 61, no. 1, p. 239.
24. Boreskov, G.K., *Geterogennyi kataliz* (Heterogeneous Catalysis), Moscow: Nauka, 1986, p. 195.
25. Popovskii, V.V., Sazonov, V.A., Chermoshentseva, G.K., *et al., Mater. III Vsesoyuz. konfer. "Kataliticheskaya ochistka otkhodyashchikh gazov promyshlennykh predpriyatii i vykhlopnykh gazov avtotransporta"* (Proc. of III All-Union Conf. on Cleaning of Exhaust Gases from Industrial Enterprises and Cars), Novosibirsk: Inst. of Catalysis, 1981, ch. 1, p. 80.